An Eigenvalue Perturbation Solution for the Multi-Physics Simulation of Antenna Strain Sensors

Chunhee Cho*, Xiaohua Yi*, Dan Li, Yang Wang, Member, *IEEE*, Manos M. Tentzeris, Fellow, *IEEE*

***Abstract*—To simulate the behavior of a passive antenna strain sensor, current multi-physics coupled simulation (between mechanics and electromagnetics) has mainly adopted the frequency domain solution. For every frequency point in the sweeping range, the frequency domain solver computes the value of scattering parameter S_{11}. The S_{11} curve is used to identify the new resonance frequency when the antenna sensor is at certain strain level. As a result, the frequency domain solution is computationally expensive. In this study, an eigenfrequency solution, whose efficiency is shown to be much higher than the frequency domain solver, is proposed to directly detect changes of antenna resonance frequency under strain. Towards the eigenfrequency solution, cavity and partially air-filled cavity FEM modeling techniques are proposed to reduce the number of degrees of freedom. In addition, by formulating the eigenfrequency solution as an eigenvalue perturbation problem, Rayleigh quotient iteration (RQI) and the inverse power iteration method with Rayleigh quotient (IPIRQ) are proposed to further improve the computational efficiency. The proposed methods will greatly improve the efficiency of antenna sensor designs.**

***Index Terms*— Multi-physics simulation, eigenvalue perturbation, antenna sensor, air-filled cavity, Rayleigh quotient iteration, inverse power iteration method.**

I. Introduction

Among the great variety of structural health monitoring (SHM) technologies, passive wireless sensing has obvious advantages. A passive (battery-free) wireless sensor requires neither cable nor external power supply for operation [1-5]. There are two categories of passive wireless sensing technologies for strain and crack sensing. The first one utilizes resonating circuits consisting of inductors, capacitors, and resistors [6-8]. In this category, the sensor interrogation is achieved by inductive coupling, a near field effect. Therefore, the wireless interrogation distance is usually limited to a few inches, which is inconvenient for practical applications. The second category relies on far field effect to characterize changes in antenna properties, including resonance frequency, power spectrum, and return loss [9-11]. When an antenna experiences strain deformation, the antenna shape changes, causing shift in electromagnetic resonance frequency of the antenna. For example, authors have developed passive RFID (radio frequency identification) antenna sensors for wireless strain measurement [12, 13]. Through signal modulation by an economic RFID chip (costing about $0.10), the RFID antenna sensors achieve much longer interrogation distances than inductive coupling sensors, and demonstrate promising performance for wireless strain/crack sensing. In another example, a frequency doubling technique is introduced as an alternative approach for signal modulation of a passive antenna sensor [14, 15].

In order to accurately describe the electromagnetic behaviors of these antenna sensors under strain, it is essential to consider two physical domains: electromagnetics (antenna resonance frequency) and mechanics (strain) [16]. In the multi-physics simulation, the mechanical simulation is conducted for a certain strain level first. The deformed shape of the antenna structure is directly used for electromagnetic simulation through moving meshes, which transfer the actual deformed shape to the electromagnetic simulation. The resonance frequency of an antenna is determined by sweeping through a large frequency range and identifying the minimum point from the scattering parameter (S_{11}) plot. During the final stage of a sensor design, the frequency-domain simulation is necessary for verifying antenna radiation performance. Although frequency-domain simulation is a common practice, it is time consuming and inefficient, particularly when the performance of an antenna sensor needs to be characterized at many strain levels. In this study, an eigenfrequency solution is proposed to directly detect resonance frequency change of an antenna sensor under strain, without the time consuming computation of S_{11} plot at many different strain levels. The eigenfrequency solution significantly reduces simulation time while maintaining the simulation accuracy for strain sensing. In addition, two novel approaches are proposed to further improve simulation speed in this paper, one through the simulation model and the other through eigenfrequency solver.

In FE modeling of electromagnetics, a full-wave model is generally used because it can describe not only resonance frequencies but also other antenna parameters. These include antenna gain, as well as electric and magnetic radiations in near

This material is based upon work supported by the Air Force Office of Scientific Research (FA9550-14-1-0054). Any opinions, findings, and conclusions or recommendations expressed in this publication are those of the authors and do not necessarily reflect the view of the sponsor.

*The first two authors are co-first authors.

Chunhee Cho is with School of Civil and Environmental Engineering, Georgia Institute of Technology, Atlanta, GA 30332 USA. (e-mail: ccho37@gatech.edu).

Xiaohua Yi was with School of Civil and Environmental Engineering, Georgia Institute of Technology (current address: ExxonMobil Upstream Research Company at Houston, TX 77389; e-mail: yixhzju@gmail.com).

Dan Li is with School of Civil and Environmental Engineering, Georgia Institute of Technology, Atlanta, GA 30332 USA. (e-mail: dli323@gatech.edu).

Yang Wang is with School of Civil and Environmental Engineering, Georgia Institute of Technology, Atlanta, GA 30332 USA. (e-mail: yang.wang@ce.gatech.edu).

Manos M. Tentzeris is with School of Electrical and Computer Engineering, Georgia Institute of Technology, Atlanta, GA 30332 USA (e-mail: etentze@ece.gatech.edu).

and far fields. However, the full-wave model is computationally expensive because oftentimes hundreds of thousands of degrees of freedom (DOFs) are needed for accuracy [12, 15, 16]. In this paper, the cavity and partially air-filled cavity models are proposed to reduce the number of DOFs from a full-wave model [17, 18]. The cavity model reduces computational loads by simply removing the air volume, and thus, all air elements. For the partially air-filled cavity model, although an air domain still exists, the size of the air box is much smaller than the air volume of the full-wave model. In the boundary conditions to truncate the simulation domain, while the full-wave model commonly uses perfectly matched layers (PMLs) to require several mesh layers, both new models use perfect electric conductor (PEC) and perfect magnetic conductor (PMC) to be defined by only one layer. As a result, the proposed eigenfrequency solution with cavity or partially air-filled cavity model requires order-of-magnitude less computing time compared with the common approach of simulating S_{11} plots of a full-wave model at multiple strain levels. This paper will also examine the accuracy of the proposed models and eigenfrequency solution.

In order to further improve computing speed in antenna sensor design, this paper also investigates a number of eigenvalue perturbation algorithms for finding eigenfrequency at a new strain level. As the antenna sensor deforms under strain, the finite element model computes deformed geometries to generate the new inductance and capacitance matrices of the antenna. The eigenfrequency algorithms utilize results from a previous step as a starting point, viewing the eigenvalue problem at the next strain level as a small perturbation to the previous strain level. Based on the commonly used Rayleigh quotient iteration (RQI) method, we propose an inverse power iteration method with Rayleigh quotient (IPIRQ) [19-21]. Rapid solution of the eigenvalue problem provides the shifted resonance frequency of the antenna sensor at the new strain level. These proposed eigenvalue perturbation algorithms allow the resonance frequencies of the antenna sensor to be rapidly identified at many strain levels. As a result, the strain sensitivity of the antenna sensor can be immediately calculated as the slope of the (approximately) linear relationship between resonance frequency and strain level.

The rest of this paper is organized as follows. Section II describes finite element formulation of the eigenfrequency (eigenvalue) problem for antenna sensors. Section III compares the computing load and accuracy of three FEM electromagnetic models, including full-wave, cavity, and partially air-filled cavity models. Section IV presents RQI and IPIRQ techniques. Section V shows a validation example of the proposed methods with a 2.9GHz patch antenna. Finally, the paper is summarized with a conclusion and future work.

II. Finite Element Formulation of the Eigenvalue Problem

This section describes the finite element formulation and its eigenfrequency solution of antenna sensors. Section A introduces the basic finite element formulation in electromagnetic problems. Section B presents the eigenfrequency solution from state-space formulation. Section C compares the simulation efficiency of the eigenfrequency solution and the frequency domain solution.

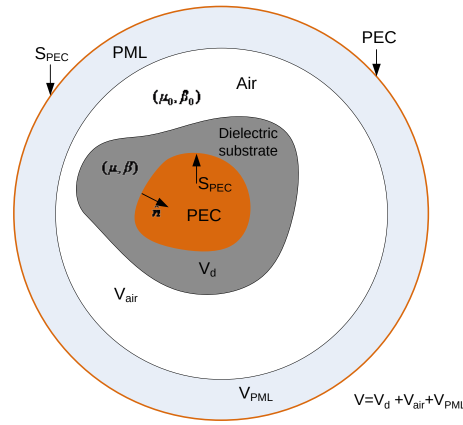

Fig. 1. Inhomogeneous structure enclosed by termination boundaries

A. Finite element formulation

For simulating an antenna strain/crack sensor, Fig. 1 illustrates the domains including the sensor, an air sphere, and PML. A patch antenna sensor usually includes a top metallic surface, a dielectric substrate layer in the middle, and a bottom ground plane for attaching to the structure being monitored. The substrate material affects antenna radiation performance and antenna size. The metallic surface is usually modeled as PEC materials. The boundary of the metallic surface is denoted as S_{PEC}, whose direction is $\hat{n}$. The volume of the dielectric substrate is denoted as V_d and the substrate relative permittivity and permeability are μ_r and β_r, respectively. The entire antenna sensor is placed inside an air sphere, whose permittivity and permeability are μ_0 and β_0, respectively. Since a resonant antenna model is an open structure that has no definite physical boundaries, it is necessary to set termination boundaries so that the simulation domain is finite. The combination of PML and PEC is adopted in the 3D electromagnetic simulation. The Maxwell's equations in an inhomogeneous material have the general vector form [22, 23]:

$$\begin{aligned} \nabla \times \mathbf{E} &= -j\omega\mu\mathbf{H} \\ \nabla \times \mathbf{H} &= j\omega\beta\mathbf{E} + \mathbf{J} \\ \nabla \cdot (\beta\mathbf{E}) &= \rho \\ \nabla \cdot (\mu\mathbf{H}) &= 0 \end{aligned} \tag{1}$$

where $\mathbf{E} = E_x\hat{\mathrm{x}} + E_y\hat{\mathrm{y}} + E_z\hat{\mathrm{z}}$ is the electric field; $\mathbf{H} = H_x\hat{\mathrm{x}} + H_y\hat{\mathrm{y}} + H_z\hat{z}$ is the magnetic field; $\mathbf{J}$ is the current vector; ρ is charge density; μ and β are the permeability and permittivity of the material, respectively; ω is the angular frequency; ∇ is the del operator in Cartesian coordinates:

$$\nabla = \hat{\mathrm{x}}\frac{\partial}{\partial \mathrm{x}} + \hat{\mathrm{y}}\frac{\partial}{\partial \mathrm{y}} + \hat{\mathrm{z}}\frac{\partial}{\partial \mathrm{z}} \tag{2}$$

In finite element method, the entire solution domain is discretized into a finite number of elements. Each element occupies a separate volume V^e (e = 1, 2, …, N_T), where N_T is the total number of elements. The electric field can then be denoted in a vector form in terms of the polynomial basis functions $\mathbf{N}_i^e$ over a general m-edge finite element [22]:

$$\mathbf{E}^e = \sum_{i=1}^{m} E_i^e \mathbf{N}_i^e \tag{3}$$

where $\mathbf{N}_i^e$ is the i-th edge based vector basis function of element e; m is the total edge number of one element; E_i^e is the tangential electric field along the i-th edge of element e. According to variational principle, the following discretized equation can be obtained [24]:

$$(j\omega)^2 \sum_{e=1}^{\mathrm{N_T}} [T^e]\{E^e\} + (j\omega) \sum_{e=1}^{\mathrm{N_T}} [R^e]\{E^e\} + \sum_{e=1}^{\mathrm{N_T}} [C^e]\{E^e\} = \sum_{e=1}^{\mathrm{N_T}} \{p^e\} \tag{4}$$

where μ is the permeability; ω is angular frequency; $[C^e]$, $[R^e]$ and $[T^e]$ are elementary inductance, damping, and capacitance matrix, respectively; p^e is the source term due to incident voltage or current excitation at the port. The entries of the matrix, $[C^e]$, $[R^e]$and $[T^e]$ are given by

$$C_{ij}^e = \int_{V^e} \frac{1}{\mu} (\nabla \times \mathbf{N}_i^e) \cdot (\nabla \times \mathbf{N}_j^e)\, dv$$
$$R_{ij}^e = \mu \left[\iint_{S^e} \mathbf{N}_i^e \cdot (\hat{n} \times \mathbf{N}_j^e) dS \right] \tag{5}$$
$$T_{ij}^e = \int_{V^e} \beta \mathbf{N}_i^e \cdot \mathbf{N}_j^e\, dv$$

where V^e is the volume of element e; S^e is the boundary of element e.

B. *Eigenfrequency solution*

If no excitation is considered, the source term $\{p^e\}$ in Eq. (4) vanishes. The equation can be rewritten as [22] with simplification:

$$\lambda^2 [\mathrm{T}]\{\mathrm{E}\} + \lambda [\mathrm{R}]\{\mathrm{E}\} + [\mathrm{C}]\{\mathrm{E}\} = \{0\} \tag{6}$$

where λ is eigenvalue; [C] is named as inductance matrix; [T] is named as capacitance matrix, while [R] is the damping matrix. The final formulation in Eq. (6) ends up as a quadratic eigenvalue problem [25, 27]. Using N to denote the total number of degrees of freedom in Eq. (6), [C] and [R] are N × N complex symmetric matrices, while [T] is an N × N real symmetric matrix. Since the entry T_{ij}^e in Eq. (5) includes material permittivity β, which is a small number on the order of 10^{-12}, the magnitudes of T_{ij}^e as well as entries in global matrix [T] are small. The entry R_{ij}^e in Eq. (5) is also small due to small magnitude of μ_0. With small-magnitude entries in [R] and [T], the matrices are usually ill-conditioned. To improve the condition number of the two matrices, a scaling factor is empirically determined as follows.

$$s = 1{,}000 \times \frac{\max_{i,j} |\mathrm{C}_{i,j}|}{\max_{i,j} |\mathrm{T}_{i,j}|} \tag{7}$$

To this end, Eq. (6) is reformulated as:

$$\tilde{\lambda}^2 [\mathrm{T^s}]\{\mathrm{E}\} + \tilde{\lambda} [\mathrm{R^s}]\{\mathrm{E}\} + [\mathrm{C}]\{\mathrm{E}\} = \{0\} \tag{8}$$

where

$$[\mathrm{R^s}] = \sqrt{s}[\mathrm{R}]; \quad [\mathrm{T^s}] = s[\mathrm{T}]; \quad \tilde{\lambda} = \lambda/\sqrt{s}; \tag{9}$$

State-space formulation equivalently converts Eq. (6) into a generalized eigenvalue problem:

$$[\mathrm{A}]\{\Phi\} = \tilde{\lambda}[\mathrm{B}]\{\Phi\} \tag{10}$$

where

$$[\mathrm{A}] = \begin{bmatrix} -[\mathrm{C}] & [0] \\ [0] & [\mathrm{T^s}] \end{bmatrix}, [\mathrm{B}] = \begin{bmatrix} [\mathrm{R^s}] & [\mathrm{T^s}] \\ [\mathrm{T^s}] & [0] \end{bmatrix}, \{\Phi\} = \begin{Bmatrix} \{\mathrm{E}\} \\ \tilde{\lambda}\{\mathrm{E}\} \end{Bmatrix} \tag{11}$$

Here [0] is an N×N zero matrix.

The eigenvalue λ is closely related with resonance frequency of the antenna sensor f_{R} according to the following equation:

$$\tilde{\lambda} = \frac{\mathrm{j}\omega - a}{\sqrt{s}} = \frac{\mathrm{j}2\pi f_{\mathrm{R}} - a}{\sqrt{s}} \tag{12}$$

The resonance frequency f_{R} is a key parameter determining the strain effects of the antenna sensor. Real value a is used to determine the quality factor for antenna design. Associated with every eigenvalue λ, eigenvector $\{\Phi\}$ represents the electric field distribution of each eigenmode.

C. *Comparison of eigenfrequency and frequency domain solutions*

In order to compare performances of two solutions for strain sensing simulation, i.e. the eigenfrequency solution and the frequency domain solution, a 2.9GHz patch antenna is modeled as an example using the commercial multi-physics software package COMSOL (Fig. 2). The substrate material of the example model is Rogers RT/duriod®5880 with dielectric constant ($\varepsilon_r = 2.2$) and low loss tangent of 0.0009. The thickness of the substrate is 0.7874mm and the planar dimension of the 2.9GHz patch antenna is 44.5mm × 33.3mm. The antenna is mounted on an aluminum specimen. Strain is applied to the two ends of the aluminum specimen. The 3D full-wave electromagnetic simulation setup of the 2.9GHz

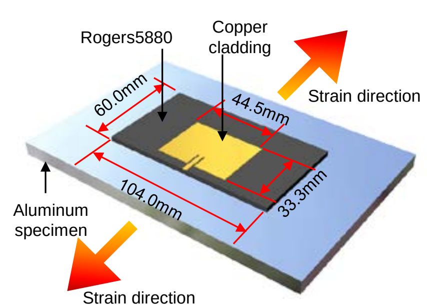

Fig. 2. Illustration of the 2.9GHz patch antenna on the aluminum specimen

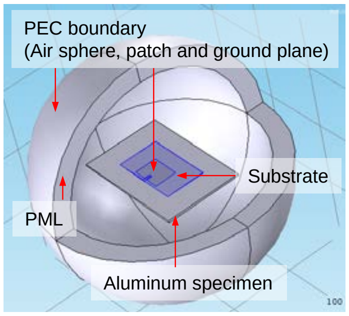

(a) Full-wave model

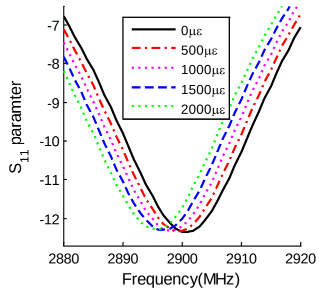

(b) S_{11} parameter (frequency domain solver)

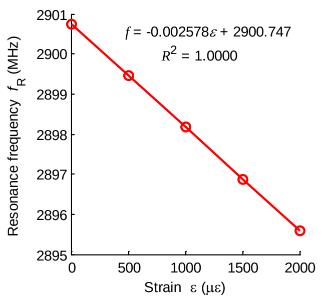

(c) Resonance frequency versus strain (frequency domain solver)

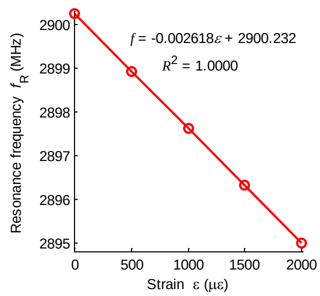

(d) Resonance frequency versus strain (eigenfrequency solver)

Fig. 3. Comparison between frequency domain and eigenfrequency solvers in the full-wave model

model for COMSOL is presented in Fig. 3(a). PEC boundaries are assigned to the outside of the air sphere, the patch, and the ground plane. The PML boundary is also combined with the PEC at the air sphere. The total number of degrees of freedom (DOFs) is 259,975. Simulations are conducted on a desktop with Intel® Xeon® processor E5-1620V3 (four cores, 3.5GHz) and 16 GB RAM memory.

At first, the frequency domain solver simulates a scattering parameter S_{11} plot (Fig. 3(b)). This is an indicator of the antenna radiation performance in the sweeping frequency ranges at different strain levels from zero to 2,000με, with 500με strain increase per step. The computation of S_{11} curve at each strain level is performed for 51 frequency points, consuming 9,722 seconds (2hours, 42 minutes, 2 seconds) in total. The minimum valley point of a S_{11} plot presents the resonance frequency of the antenna at that strain level. As a post processing procedure, linear regression is performed between resonance frequency and strain to construct the strain sensitivity plot (Fig. 3(c)). The resonance frequency is 2,900.75MHz and strain sensitivity is –2,578Hz/με, which means 1με strain experienced by the patch antenna introduces a frequency change of –2,578Hz. The coefficient of determination is close to 1.0000, which shows a highly linear relationship.

In the eigenfrequency solution, COMSOL LiveLink™ interface for MATLAB is adopted [28]. The mechanics simulation for certain strain level is conducted first in the mechanical domain. Through the LiveLink™, the [C], [R], and [T] from COMSOL are transferred into the MATLAB, which formulates [A] and [B] matrix (Eq. (10) and (11)). Finally MATLAB `eigs` command is used to compute the generalized eigenvalue solution of these sparse [A] and [B] matrix [28]. The `eigs` command is set to directly search the eigenfrequency close to 2900MHz. The eigenfrequency is again extracted for each strain level. After performing linear regression between resonance frequency and strain data, the strain sensitivity is identified as –2,618Hz/με and resonance frequency at zero strain level is 2900.23MHz (Fig. 3 (d)). These are very close to the frequency-domain results. The coefficient of determination is also rounded off to 1.0000. The computing time at each strain level is 520 seconds (8 min 40 seconds) for the eigenfrequency solver, which is much faster than the frequency-domain solver. Therefore, it is demonstrated that the strain sensitivity simulation, the efficiency of the eigenfrequency solver is nearly 20 times higher than the frequency-domain solver.

III. FEM Modeling Techniques to Improve Simulation Efficiency

This section describes two electromagnetic FEM modeling techniques to reduce computational efforts with much less number of DOFs. Section A presents a cavity model, which removes the air volume from the full-wave model to reduce DOFs. However, it was observed that the cavity model cannot consider fringing effect due to the lack air volume. In order to address this problem, Section B describes a partially air-filled cavity model which has a shallow air box on the patch antenna to compensate the fringing effect, without significantly increasing the number of DOFs.

A. Cavity model

Although the eigenfrequency solution in the full-wave model provides similar results as the frequency-domain results, many spurious modes exist along with the resonance mode. Therefore, it can be difficult to identify the correct resonance mode and the corresponding frequency. By removing the air sphere and modifying boundary conditions correspondingly, a cavity model entails much less DOFs than the full-wave model. The cavity model of the 2.9GHz patch antenna is shown in Fig. 4(a). PEC boundaries are assigned as the microstrip patch and a ground plane. PMC boundaries are assigned to four sides and the top of the substrate. These boundary conditions exclude the aluminum plate in this electromagnetic domain simulation although the plate still exists in the mechanical simulation. Therefore, while electromagnetic domain of the full-wave model contains the aluminum plate and the air, the cavity model contains only the patch antenna and achieves faster computing. The total number of DOFs is 24,459, which is about 10 times

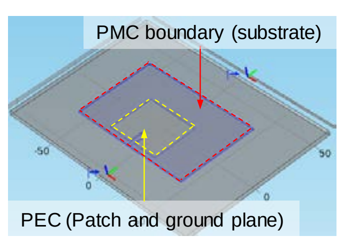

(a) Cavity model

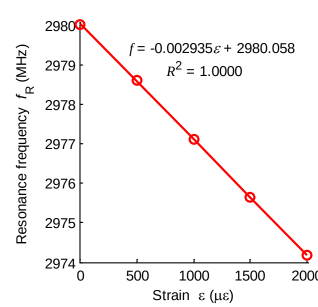

(b)Resonance frequency versus strain

Fig. 4. Cavity model simulation

smaller than that of the full-wave model.

Benefiting from much less DOFs, total computing time of the eigenfrequency solver at each strain level is only 8 seconds. However, because PMC boundary conditions are assigned on the substrate, a fringing field is not generated around the side of the microstrip patch in the cavity model. Therefore, the simulated resonance frequency at zero strain is 2980.06MHz (Fig. 4(b)), which is 2.7% different from resonance frequency of the full-wave model in Section II. Fig. 4(b) shows the simulated strain sensitivity to be –2,935Hz/με, which is also 12.1% higher than the full-wave model. In conclusion, although the cavity model requires less computation, this approach has notable inaccuracy because of neglecting the fringing effect.

B. Partially air- filled cavity model

By adding a small air box to the cavity model, the fringing field is restored in the electromagnetics simulation. Fig. 5 explains the electric field comparison between a cavity and a partially air-filled cavity model. The cavity model assigns PMC boundaries on the surface of the substrate, which blocks the generation of the electric field in the horizontal direction. In other words, the direction of the electrical field is only vertical

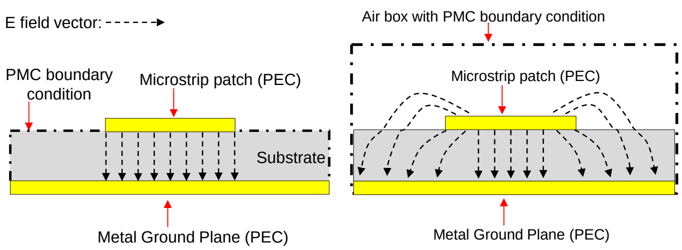

(a) Cavity model (b) Partially air-filled cavity model

Fig. 5. Electric field comparison

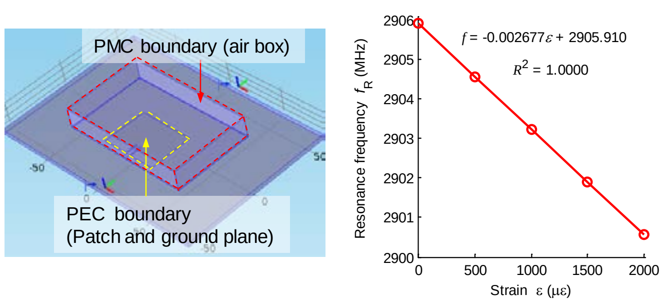

(a) Partially air-filled cavity model (b)Resonance frequency versus strain

Fig. 6. Partially air-filled cavity model simulation

Table 1. Comparison of three FEM models

	Full-wave model	Cavity model	Partially air-filled cavity model
Resonance frequency	2900.23MHz	2980.06MHz (*error: 2.75%)	2905.91MHz (*error: 0.20%)
Strain sensitivity	–2,618Hz/με	–2,935Hz/με (*error:12.12%)	–2,677Hz/με (*error: 2.25%)
No. of DOFs	259,975	24,459	56,379
Eigenfrequency solution time at each strain level	520 seconds	8 seconds	25 seconds

* Errors are relative to the full wave model

(Fig. 5(a)). The partially air-filled cavity model assigns PMC boundary conditions on the added air box, which provides enough space for generating the horizontal electrical field (Fig. 5(b)). Therefore, the partially air-filled cavity model is able to describe the fringing field.

The partially air-filled cavity model of the 2.9GHz patch antenna is simulated in COMSOL (Fig. 6). PEC boundary conditions are the same as in the cavity model in Section A, and PMCs are assigned on the surface of the air box (Fig. 6(a)). The number of DOFs is 56,379. Although this number is larger than that of the cavity model, it is still five times smaller than the full-wave model. As shown in Fig. 6(b), simulated resonance frequency is 2905.91 MHz, which is much closer to the resonance frequency from the full wave model. Strain sensitivity is calculated as –2,677Hz/με and the coefficient of determination is close to 1.0000. The computing time at each strain level of the eigenfrequency solver is 25 seconds. The comparison among three FEM models in Section II-III is briefly summarized in Table 1. The partially air-filled cavity model is shown to achieve the best trade-off between computing time and accuracy.

IV. Eigenfrequency Solvers for Strain Sensing Simulation

In the strain sensing simulation, because changes of system matrices [A] and [B] between two adjacent strain levels are expected to be small, the differences in eigenfrequencies and eigenvectors are likewise small. In order to reach fast convergence, the eigenvalues and eigenvectors in the previous step can be utilized as starting vectors to search for solution at the next strain step. Section A explains the Rayleigh quotient iteration (RQI) method, a commonly used eigenvalue algorithm. In Section B, we proposed an inverse power iteration with Rayleigh quotient (IPIRQ) method which can be implemented to further improve the solution speed. Section 0 describes the overall COMSOL-MATLAB framework for strain sensing simulation using these eigenvalue perturbation algorithms.

A. Rayleigh Quotient Iteration (RQI) method

The Rayleigh quotient iteration (RQI) method is implemented to improve computational efficiency of the eigenfrequency solution. To find the interested eigenfrequency of an antenna resonance mode, the shifted version of RQI is implemented (Fig. 7).

As described in Eq. (11), [A] and [B] are complex-valued symmetric and sparse matrices. Since matrix with a smaller bandwidth generally improves speed of linear solvers, the reverse Cuthill-McKee algorithm [29] is applied to [A] and [B] first in step ①, producing a preordering permutation matrix [P] and preordered matrices $[\widetilde{A}_{j+1}]$ and $[\widetilde{B}_{j+1}]$ with smaller bandwidth. In step ②, since the generalized eigenvalue is not affected by the preordering process, λ_j at strain level ε_j is directly saved as an intermediate eigenvalue μ for starting the search. Meanwhile, the starting eigenvector $\{q\}$ is determined by reordering eigenvector $\{\Phi_j\}$ with permutation matrix [P]. In step ③, a temporary scaler d is computed once for later repetitive use in the `do-while` loop. In step ④, the LU factorization is performed with $[\widetilde{A}_{j+1}] -$

① Preordering $[\mathrm{P}][\mathrm{A}_{j+1}][\mathrm{P}]^{\mathrm{T}} = [\tilde{\mathrm{A}}_{j+1}]$;
$[\mathrm{P}][\mathrm{B}_{j+1}][\mathrm{P}]^{\mathrm{T}} = [\tilde{\mathrm{B}}_{j+1}]$;

② $\mu = \lambda_j$; $\{q\} = [\mathrm{P}]\{\Phi_j\}$;

③ $d = \|[\tilde{\mathrm{A}}_{j+1}]\| + \|\mu[\tilde{\mathrm{B}}_{j+1}]\|$;

do {

④ LU factorization $([\tilde{\mathrm{A}}_{j+1}] - \mu[\tilde{\mathrm{B}}_{j+1}]) = [\mathrm{L}][\mathrm{U}]$;

⑤ $\{q\} = [\mathrm{U}^{-1}][\mathrm{L}^{-1}][\tilde{\mathrm{B}}_{j+1}]\{q\}$;

$\{q\} = \dfrac{\{q\}}{\|\{q\}\|}$;

⑥ $\mu = \dfrac{\{q\}^{\mathrm{H}}[\tilde{\mathrm{A}}_{j+1}]\{q\}}{\{q\}^{\mathrm{H}}[\tilde{\mathrm{B}}_{j+1}]\{q\}}$;

⑦ error $= \dfrac{\|[\tilde{\mathrm{A}}_{j+1}]\{q\} - \mu[\tilde{\mathrm{B}}_{j+1}]\{q\}\|}{d}$;

} while (error > tolerance);

⑧ $\lambda_{j+1} = \mu$; $\{\Phi_{j+1}\} = [\mathrm{P}]^{\mathrm{T}}\{q\}$;

Fig. 7. RQI routine for shifted symmetric [A] and [B] formulations

$\mu[\tilde{\mathrm{B}}_{j+1}]$ to obtain a lower triangular matrix [L] and upper triangular matrix [U]. This LU factorization is the most computationally expensive step in RQI process. In step ⑤, the intermediate eigenvector $\{q\}$ is updated and normalized. In step ⑥, the intermediate eigenvalue μ is updated by the Rayleigh quotient. In step ⑦, the error of the current step is calculated. If the error is lower than tolerance, the loop terminates; the eigenvalue λ_{j+1} and eigenvector $\{\Phi_{j+1}\}$ at strain level ε_{j+1} are updated in step ⑧. To restore the original eigenvector order, the intermediate eigenvector $\{q\}$ is reordered by the transpose of the permutation matrix $[\mathrm{P}]^{\mathrm{T}}$. If the error is higher than tolerance, the algorithm returns to step ④ and iterates the process.

B. *Inverse Power Iteration with Rayleigh Quotient (IPIRQ) method*

Although the RQI method is commonly used, an Inverse power iteration with Rayleigh quotient (IPIRQ) method is proposed to herein further improve computing speed. In the RQI method, the most computationally expensive step is the LU factorization. When the RQI method iterates in the `do-while` loop, the LU factorization is computed in every iteration, increasing computational loads. In comparison, the proposed IPIRQ method performs the factorization only one time and effectively reuses factorization results ([L] and [U] matrices) for each iteration. Therefore, the IPIRQ method can be much faster than the RQI method in most cases [21].

The process of the IPIRQ from step ① to ③ is the same as the RQI method in Fig. 7. But, in step ④, the LU factorization is moved out of the `do while` loop, and placed before `do`. The process from step ⑤ to ⑧ also follows the RQI method. Compared with the RQI method, the [L] and [U] matrices used at step ⑤ of the IPIRQ method are only accurate at first iteration. At the second or any later iteration, the RQI performs factorization to $[\tilde{\mathrm{A}}_{j+1}] - \mu[\tilde{\mathrm{B}}_{j+1}]$ with the updated μ value, to get updated [L] and [U]. However, IPIRQ reuses the [L] and [U] from the first iteration as approximation to these two matrices at the current iteration. Therefore, despite time saving, the accuracy of IPIRQ is yet to be examined.

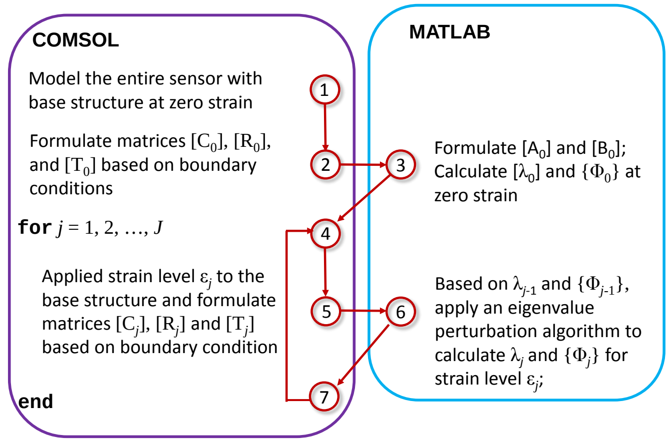

Fig. 8. COMSOL-MATLAB communication

C. *COMSOL-MATLAB framework*

The antenna sensor models can be easily built in COMSOL through user friendly graphical interface, but it is not convenient to implement customized eigenvalue solvers into COMSOL graphical interface. Instead, COMSOL LiveLink for MATLAB allows the customized solvers to be applied to COMSOL-generalized matrices in electromagnetic domain.

Fig. 8 shows the COMSOL-MATLAB communication process using eigenvalue techniques for updating sensor resonance frequencies at multiple strain levels. The simulation model is first built in COMSOL with proper mechanical and electromagnetic boundary conditions. Matrices $[\mathrm{C}_0]$, $[\mathrm{R}_0]$, and $[\mathrm{T}_0]$ in Eq. (6) are then generated by COMSOL and transferred to MATLAB. These matrices are used to construct $[\mathrm{A}_0]$ and $[\mathrm{B}_0]$ according to Eq. (11). The eigenvalue λ_0 and eigenvector $\{\Phi_0\}$ are calculated through eigenvalue solver at zero strain level ε_0.

Upon the simulation at zero strain level and later at a *j*-th strain level, the antenna structure is subjected to corresponding loading in COMSOL. The deformed antenna shape is used to generate inductance and capacitance matrices at strain level ε_j. The corresponding system matrices $[\mathrm{A}_j]$ and $[\mathrm{B}_j]$ are constructed in MATLAB. An eigenvalue perturbation algorithm can then be applied to calculate the eigenvalue λ_j and eigenvector $\{\Phi_j\}$ at strain ε_j, based on λ_{j-1} and $\{\Phi_{j-1}\}$ from the previous strain step. The updating process continues for all required strain levels.

V. VALIDATION EXAMPLE

To validate the accuracy and efficiency of the proposed partially air-filled cavity model and the IPIRQ eigenvalue perturbation algorithm, the same 2.9GHz patch antenna is investigated. Four strain levels are simulated, ranging 500~2,000 με with a strain step of 500 με. The eigenfrequency at each strain level is first calculated by `eigs` function in MATLAB. To check the effect of different starting vectors to the computation error and time, a randomly generated vector and the eigenvector from previous strain level are adopted as the starting vector, respectively for comparison. The RQI and the IPIRQ methods are applied for comparison with the two MATLAB eigs solutions with different starting vectors. The error tolerance for the four methods (two eigs, RQI, and IPIRQ) is set to 10^{-16}.

The computed resonance frequency results from the four solvers are compared and summarized in Fig. 9. The legend "eigs-rand" denotes the results from eigs function with randomly generated vector as starting vector; the legend "eigs-prev" indicates results from eigs function with previous eigenvector as starting vector; the legend "RQI" and "IPIRQ" denote the results from the RQI and the IPIRQ methods, respectively. In this example, the resonance frequencies from four solution methods show good match (Fig. 9(a)) at all strain steps. Fig. 9(b) shows the closed-up view at 1,000 με.

To further compare the solution accuracy, following error index is defined:

$$\text{error} = \frac{\left\| \mathrm{A}_{j+1}\{\Phi_{j+1}\} - \lambda_{j+1}\mathrm{B}_{j+1}\{\Phi_{j+1}\} \right\|}{\left\| \mathrm{A}_{j+1} \right\| + \left\| \lambda_{j+1}\mathrm{B}_{j+1} \right\|} \tag{13}$$

where λ_{j+1} and $\{\Phi_{j+1}\}$ are the computed eigenvalue and eigenvector at (j+1)-th strain step.

As shown in Fig. 9(c), the computational errors of all methods are lower than 1×10^{-16}. Computation error for the RQI and the IPIRQ methods is between 3.8×10^{-18} to 4.2×10^{-18}, both smaller than the `eigs` solutions. Comparison of computation time is plotted in Fig. 9(d). The computation time of IPIRQ is the fastest, which is about 1.3 times faster than the `eigs` solutions and 1.86 times faster than the RQI method. To explain the difference between RQI and IPIRQ, Table 2 provides computation time for every step of these two methods at 1,000με level. The step numbers follow Fig. 7. As shown in the table, a critical time-consuming step of both algorithms is LU factorization (Step ④ in both methods). Therefore, although RQI has only two iterations and IPIRQ needs three iterations to converge, IPIRQ is more efficient than RQI by reusing LU factorization while achieving similar accuracy.

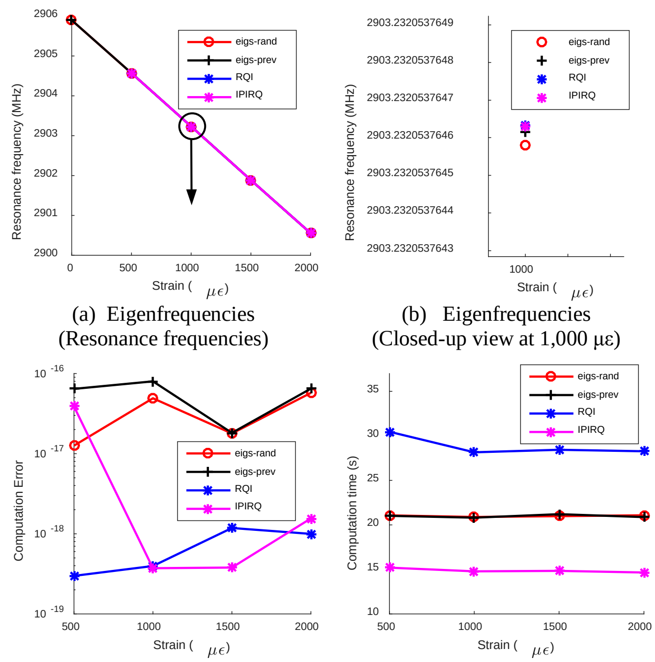

(a) Eigenfrequencies (Resonance frequencies)

(b) Eigenfrequencies (Closed-up view at 1,000 με)

(c) Computation error

(d) Computation time

Fig. 9. Eigenfrequency results comparison between `eigs` solvers and proposed method

Table 2. Computation time (seconds) of RQI and IPIRQ at 1000 με

Step	RQI		IPIRQ		
①	0.1802		0.1923		
②	0.0012		0.0014		
③	0.3923		0.4170		
	First iteration	Second iteration			
④	13.4173	13.6476	13.4474		
			First iteration	Second iteration	Third iteration
⑤	0.2135	0.2072	0.2020	0.1855	0.1974
⑥	0.0127	0.0113	0.0124	0.0102	0.0101
⑦	0.0338	0.0384	0.0399	0.0372	0.0334

Summary and Discussion

This study first presents electromagnetic finite element formulation of antenna sensors using both frequency domain solver and eigenfrequency solver. The 2.9 GHz patch antenna simulation is performed using both solvers, and the calculated resonance frequency results are compared. The eigenfrequency solver consumes nearly 5% of the time required by the frequency-domain solver, while providing the similar accuracy.

In order to reduce computational loads, two FEM models (cavity and partially air-filled cavity models) are proposed. While the cavity model significantly reduces simulation time, the accuracy is not reliable due to the absence of air volume. It is discovered that the partially air-filled cavity model not only reduces computational efforts but also maintains accuracy for the electromagnetic simulation. To further improve the solution efficiency, two eigenvalue perturbation methods, RQI and IPIRQ are studied. The solution accuracy and efficiency are compared with MATLAB `eigs` command. The results show that the commonly used RQI method achieves high computation accuracy, but it is relatively slower than other solutions. Meanwhile, the proposed IPIRQ method achieves the best balance between accuracy and timing.

Overall, the proposed antenna simulation approach, using partially air-filled model and the IPIRQ eigenvalue perturbation method, provides an eigenvalue solution in 14.82 seconds for the 2.9GHz antenna at 1,000 με. In comparison, the conventional frequency domain solver requires 9,722 seconds (2hours, 42 minutes, 2 seconds). The efficiency improvement is significant. The proposed approach provides a simulation framework enabling much more efficient antenna sensor designs.

References

[1] E. G. Straser and A. S. Kiremidjian, "*A Modular, Wireless Damage Monitoring System for Structures*," John A. Blume Earthquake Eng. Ctr., Stanford

University, Stanford, CA Report No. 128, 1998.

[2] J. P. Lynch, K. H. Law, A. S. Kiremidjian, C. E., C. R. Farrar, H. Sohn, D. W. Allen, B. Nadler, and J. R. Wait, "Design and performance validation of a wireless sensing unit for structural health monitoring applications," *Structural Engineering and Mechanics*, vol. 17(3-4), pp. 393-408, 2004.

[3] Y. Wang, J. P. Lynch, and K. H. Law, "A wireless structural health monitoring system with multithreaded sensing devices: design and validation," *Structure and Infrastructure Engineering*, vol. 3(2), pp. 103-120, 2007.

[4] J. P. Lynch and K. J. Loh, "A summary review of wireless sensors and sensor networks for structural health monitoring," *The Shock and Vibration Digest*, vol. 38(2), pp. 91-128, 2006.

[5] A. Deivasigamani, A. Daliri, C. H. Wang, and S. John, "A Review of Passive Wireless Sensors for Structural Health Monitoring," *Modern Applied Science*, vol. 7(2), pp. 57-76, 2013.

[6] J. C. Butler, A. J. Vigliotti, F. W. Verdi, and S. M. Walsh, "Wireless, passive, resonant-circuit, inductively coupled, inductive strain sensor," *Sensors and Actuators A: Physical*, vol. 102(1-2), pp. 61-66, 2002.

[7] K. J. Loh, J. P. Lynch, and N. A. Kotov, "Inductively coupled nanocomposite wireless strain and pH sensors," *Smart Structures and Systems*, vol. 4(5), pp. 531-548, 2008.

[8] Y. Jia, K. Sun, F. J. Agosto, and M. T. Quinones, "Design and characterization of a passive wireless strain sensor," *Measurement Science and Technology*, vol. 17(11), pp. 2869-2876, 2006.

[9] A. Daliri, A. Galehdar, S. John, C. H. Wang, W. S. T. Towe, and K. Ghorbani, "Wireless strain measurement using circular microstrip patch antennas," *Sensors and Actuators A: Physical*, vol. 184(1), pp. 86-92, 2012.

[10] S. Deshmukh and H. Huang, "Wireless interrogation of passive antenna sensors," *Measurement Science and Technology*, vol. 21(3), 2010.

[11] X. Xu and H. Huang, "Battery-less wireless interrogation of microstrip patch antenna for strain sensing," *Smart Materials and Structures*, vol. 21(12), p. 125007, 2012.

[12] X. Yi, C. Cho, J. Cooper, Y. Wang, M. M. Tentzeris, and R. T. Leon, "Passive wireless antenna sensor for strain and crack sensing-electromagnetic modeling, simulation, and testing," *Smart Materials and Structures*, vol. 22(8), p. 085009, 2013.

[13] X. Yi, T. Wu, Y. Wang, R. T. Leon, M. M. Tentzeris, and G. Lantz, "Passive wireless smart-skin sensor using RFID-based folded patch antennas," *International Journal of Smart and Nano Materials*, vol. 2(1), pp. 22-38, 2011.

[14] X. YI, C. Cho, J. Cooper, R. Vyas, Y. Wang, M. M. Tentzeris, and R. T. Leon, "Passive frequency doubling antenna sensor for wireless strain sensing," in *Proceeding of the ASME 2012 Conference on Smart Materials, Adaptive Structures and Intelligent Systems (SMASYS 2012)*, Stone Mountain, GA, USA, 2012.

[15] C. Cho, X. Yi, D. Li, Y. Wang, and M. M. Tentzeris, "Passive wireless frequency doubling antenna sensor for strain and crack sensing," *Sensors Journal, IEEE*, vol. 16(14), pp. 5725-5733, 2016.

[16] X. Yi, Y. Wang, M. M. Tentzeris, and R. T. Leon, "Multi-physics modeling and simulation of a slotted patch antenna for wireless strain sensing " in *Proceedings of the 9th International Workshop on Structural Health Monitoring (IWSHM)*, Stanford, CA, USA, 2013.

[17] K. R. Carver and J. M. Mink, "Microstrip antenna technology," *IEEE Trans. Antennas Propagation*, vol. AP-27(1), pp. 2-24, 1981.

[18] P. Daly, "Hybrid-mode analysis of microstrop by finite-element methods," *IEEE Trans. Microwave theory technology*, vol. MTT-19(19-25), 1971.

[19] B. N. Parlett, "The rayleigh quotient iteration and some generalizations for nonnormal matrices," *Mathematics of Computatoin*, vol. 28(127), pp. 679-693, 1974.

[20] A. Amiraslani and L. P., "Rayleigh quotient algorithms for nonsymmetric matrix pencils," *Numerical Algorithms*, vol. 51, pp. 5-22, 2009.

[21] J. H. Wilkinson, "*The Algebraic Eigenvalue Problem*." Oxford: Clarendon Press, 1965.

[22] J. M. Jin, "*The Finite Element Method in Electromagnetics*," 2nd ed. New York: John Wiley & Sons, Inc., 2002.

[23] W. C. Chew and W. H. Weedon, "A 3-D perfectly matched medium from modified Maxwell's equations with stretched coordinates," *Microwave and Optical Technology Letters*, vol. 7(13), pp. 599-604, 1994.

[24] J. L. Volakis, A. Chatterjee, and L. C. Kempel, "*Finite Element method for Electromagnetics: with Applications to Antenna, Microwave Circuits, and Scattering*." New York, NY: The Institute of Electrical and Electronics Engineers, Inc., 1998.

[25] H. Guo, B. Oswald, and P. Arbenz, "3-dimensional eigenmodal analysis of plasmonic nanostructures," *Optics Express*, vol. 20(5), pp. 5481-5500, 2012.

[26] A. Chatterjee, J. M. Jin, and J. L. volakis, "Edge-based finite elements and vector ABC's applied to 3-D scattering," *IEEE Transactions on Antennas and Propagation*, vol. 41(2), pp. 221-226, 1993.

[27] F. Tisseur and K. Meerbergen, "The quadratic eigenvalue problem," *SIAM Review*, vol. 43(2), pp. 235-286, 2001.

[28] T. G. Wright and L. N. Trefethen, "Large-scale computation of pseudospectra using ARPACK and eigs," *Journal of Scientific Computing*, vol. 23(2), pp. 591-605, 2001.

[29] J. A. George and J. W.-H. Liu, "*Computer Solution of Large Sparse Positive Definite Systems*." Hanford, CA: Prentice-Hall, 1981.